

15. ORIGIN AND NATURE OF GREEN CLAY LAYERS, ODP LEG 184, SOUTH CHINA SEA¹

Federica Tamburini,^{2,3} Thierry Adatte,³ and Karl B. Föllmi³

ABSTRACT

Green clay layers are reported from the Pliocene–Holocene intervals in five of the six sites drilled in the South China Sea (SCS) during Leg 184. Centimeter-scale discrete, discontinuous, and bioturbated layers, constituted by stiff and porous green clays, were observed, sometimes associated with iron sulfides and pyrite. Detailed mineralogical and geochemical analyses indicate that they differentiate from the host sediments in their higher content of iron, smectite, and mixed-layered clays and lower amounts of calcite, authigenic phosphorus, quartz, and organic matter. Although no glauconite was observed, the mineralogy and geochemistry of green clay layers, along with their geometrical relation to background sediments, suggest that they most likely represent the result of the first steps of glauconitization. Correlation between green layers and volcanic ash layers was suggested for green laminae observed elsewhere in Pacific sediments but was not confirmed at SCS sites. Statistical analysis of the temporal distribution of green layers in the records of the last million years suggests that green clay layers have become more frequent since 600 ka. Only at Site 1148 does the green layer record show a statistically significant cyclicity which may be related to orbital eccentricity. A possible influence of sea level variations, related both to climatic changes and tectonism, is postulated.

¹Tamburini, F., Adatte, T., and Föllmi, K.B., 2003. Origin and nature of green clay layers, ODP Leg 184, South China Sea. In Prell, W.L., Wang, P., Blum, P., Rea, D.K., and Clemens, S.C. (Eds.), *Proc. ODP, Sci. Results*, 184, 1–23 [Online]. Available from World Wide Web: <http://www-odp.tamu.edu/publications/184_SR/VOLUME/CHAPTERS/206.PDF>. [Cited YYYY-MM-DD]

²Woods Hole Oceanographic Institution, Marine Chemistry and Geochemistry Department, MS 8, Woods Hole MA 02543, USA.

ftamburini@whoi.edu

³Institut de Géologie, Rue Emile-Argand, 11, CH-2007 Neuchâtel, Switzerland.

Initial receipt: 10 August 2001

Acceptance: 4 March 2003

Web publication: 22 July 2003

Ms 184SR-206

INTRODUCTION

During Leg 184 in the South China Sea (SCS) characteristic lithologic features, called green clay layers (GCLs) (Wang, Prell, Blum, et al., 2000), were observed in the Pliocene–Holocene intervals at five of the six drilled sites (Fig. F1; Table T1). It is not the first time that such features have been found in marine sediments. Green and purple bands were noted in sediments from Leg 130 in the Ontong Java Plateau (Lind et al., 1993), and similar layers were observed in deposits from the Rio Grande Rise (Supko, Perch-Nielsen, et al., 1977) and the Lord Howe Rise (Gardner et al., 1986). Inside the SCS, green clay granules and foraminifer tests infilled with green clays were reported from Holocene and Pleistocene sediments in the Vietnam inner and outer shelf (Markov et al., 1996).

Several hypotheses were offered to explain the nature and the origin of these layers: (1) the presence of glauconite, (2) the alteration of volcanic material, or (3) alteration of the original clay, but the question remained unanswered. A total of 22 samples (11 green clay and 11 background sediment) (Fig. F2) were collected from Ocean Drilling Program (ODP) Sites 1147 and 1148 in the SCS. Here, we present the results of a multiproxy investigation that comprises bulk and clay mineralogy, grain size, organic matter, and phosphorus sedimentary phase characterization, bulk inorganic geochemistry by X-ray fluorescence (XRF), and statistical analysis of the temporal distribution of the GCLs. The main goals of this study are to determine the nature of the GCLs, understand their genesis, and establish any possible correlation with external factors, such as sea level changes, climate variations, and tectonism.

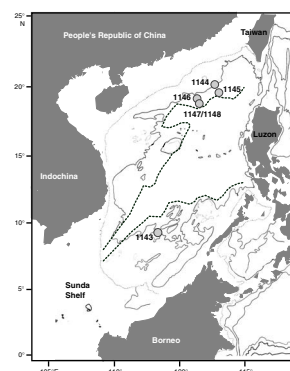
METHODS

All samples were oven dried at 50°C and divided in subsamples. Bulk sediment mineralogy was determined by X-ray diffractometry (XRD) (using a SCINTAG XRD 2000 diffractometer), based on a semiquantitative estimation and using external standards (Kübler, 1983). This method allows us to quantify a certain number of mineral species (i.e., quartz, calcite, K-feldspar, and plagioclase). Other mineral components, including amorphous minerals, Fe oxides and hydroxides, some clay minerals, and organic material cannot be quantified because of the lack of appropriate standards and technical complications (for a review, see Kübler, 1983). The relative error of the bulk rock mineralogy is ~5%.

Clay mineral analyses were based on methods by Kübler (1987). An aliquot of the sample was mixed with deionized water (pH = 7–8), and the carbonate fraction was removed by the addition of 10% HCl (1.25 N). Separation of different grain size fractions (<2 µm and 2 to 16 µm) was obtained by the timed settling method based on Stokes law. XRD analyses of oriented clay samples were made after air drying at room temperature and in ethylene glycol solvated conditions. Clay minerals for the two fractions are given in relative percent abundance. Smectite content is estimated by using the method of Moore and Reynolds (1997). The relative error does not exceed 10% of raw intensity.

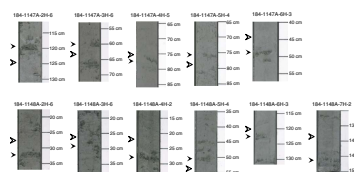
Grain size analyses were performed on the insoluble and carbonate-free residues prepared for the clay mineralogy analyses using a grain size Laser Oriel CIS (Computerized Inspection System). The relative error is 10% (Jantschik et al., 1992).

F1. Location of Leg 184 sites, p. 12.



T1. Location of Sites 1143–1148, p. 18.

F2. Samples used for this study, p. 13.



The characterization of organic matter was performed on 100 mg of dried and ground sediment with a Rock-Eval 6 and using a standard whole-rock pyrolysis method (Espitalié et al., 1986; Lafargue et al., 1996). The distribution of sedimentary phosphorus phases was determined using a four-step sequential extraction technique adapted from the SEDEX method (Anderson and Delaney, 2000; Ruttenger, 1992). For all the steps other than the iron-bound P, the ascorbic acid–molybdate blue method was employed to analyze the extracted supernatants (Greenberg, 1995). A Perkin Elmer spectrophotometer was used to determine absorbences and P concentrations. All samples were diluted 1:10 for spectrophotometric determination. Concentrations of the iron-bound P phase and ferric Fe, extracted during the first step of the procedure, were determined using an OPTIMA 3000 Perkin Elmer inductively coupled plasma–atomic emission spectrophotometer at the “Environmental Laboratory” in Neuchâtel. Typical mean errors for each phase were calculated as the relative standard deviation of the consistency standards and range from 2% to 7% for authigenic P, from 3% to 5% for detrital P, from 2% to 5% for organic P, and from 3% to 6% for iron-bound P. Because of material limitation, XRF was performed only on four selected samples at the Geological Institute of Fribourg using a sequential X-Ray spectrometer PW2400. Based on the analysis of a certified reference standard, the relative average error was $\pm 1\%$.

The depth of the GCLs was recorded during the shipboard description of the sediments directly on core description log sheets (“barrel sheets” produced by AppleCore software). The depth in meters below seafloor of each GCL at Sites 1143, 1145, 1146, 1147, and 1148 was extracted from the barrel sheets. Depths in meters composite depth and ages were calculated using the splices and the age models calculated on board and provided in Wang, Prell, Blum, et al. (2000) (see Table T2). Occurrences of GCLs from Site 1147 are analyzed together with the ones from Site 1148. Site 1147 was drilled to recover sediments that were missing or disturbed in the uppermost part of Site 1148 (Wang, Prell, Blum, et al., 2000). Tests for randomness, as well as autocorrelation and spectral analysis, were performed to investigate their temporal distribution over the last million years. All the records were resampled at even intervals and detrended before being analyzed. The Arand (by P.J. Howell, Brown University) and MatLab software packages were used.

DESCRIPTION AND RESULTS

Green clay layers are mainly concentrated in the uppermost Pliocene–Pleistocene section and, for Site 1148, in the lower Miocene section (Wang, Prell, Blum, et al., 2000). These centimeter-scale layers, consisting of generally coarser and stiffer material than background sediments, which are composed of nannofossil ooze and detrital clays, can be as thick as 3 cm and occur in high numbers, up to hundreds per core (i.e., Cores 184-1143B-12H and 184-1143C-4H) (Wang, Prell, Blum, et al., 2000). Discrete layers as well as discontinuous and bioturbated green intervals were observed (Fig. F2), and in many occurrences a clear association with iron sulfide minerals and pyrite nodules was found (Wang, Prell, Blum, et al., 2000). Smear slide analysis performed during visual inspection of the cores indicates that these layers are relatively poor in carbonate. A green mineral was recognized on smear slides and interpreted as being glauconite, but XRD analysis performed on board

T2. Depths and ages for GCLs,
p. 19.

did not validate this observation. After the plastic bags containing the sampled sediments were opened, about two months after sampling, the green color characteristic of GCLs had disappeared and the color difference between the green clay and the host sediment samples was less distinct.

Grain Size and Bulk and Clay Mineralogy

The studied sediments, both the GCL and host material, are fine grained, with material $<8 \mu\text{m}$ averaging 82%. Samples are composed of phyllosilicates, which average 17%, and quartz, which represents ~12% of the GCL and 13% of the host sediments. Other minor constituents are K-feldspar, plagioclase, and calcite, which together represent not more than 13% of bulk mineral composition. On average, ~50% of the bulk mineralogical composition of each sample is represented by the “unquantified” mineral phase (see “Methods,” p. 2) (Table T3). Small amounts of pyrite were detected in both GCLs and normal sediments (Table T3). Micas (s.l.) and chlorite constitute the most abundant clay minerals detected in the carbonate-free $<2\text{-}\mu\text{m}$ and 2- to $16\text{-}\mu\text{m}$ fractions. Micas average 52% and 49% of the $<2\text{-}\mu\text{m}$ and 2- to $16\text{-}\mu\text{m}$ fractions, respectively, whereas chlorite represents 40% and 23% of the same fractions. Kaolinite is present in lower percentages, averaging 6% and 9% of the $<2\text{-}\mu\text{m}$ and 2- to $16\text{-}\mu\text{m}$ fractions, respectively. Smectite, detected in the $<2\text{-}\mu\text{m}$ carbonate-free fraction treated with ethylene glycol, makes up ~18% of the fraction. Generally, micas are of detrital origin, as it is shown by their sharp peaks (Fig. F3).

Background sediments bear ~25% more calcite than GCLs, whereas no consequential difference in pyrite percentages was observed. GCLs are generally coarser (average = 19.3%; $>8 \mu\text{m}$) than background sediments (average = 15.1%; $>8 \mu\text{m}$). Both GCLs and background sediments contain the same amount of K-feldspar, plagioclase, and phyllosilicates, mainly chlorite and smectite (Table T3).

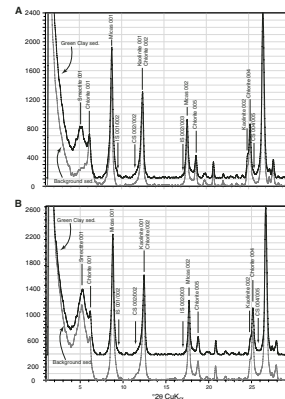
As stated by several authors (see Moore and Reynolds, 1997), the term glauconite (used for a Fe-rich mica) is “ambiguous” and the distinction between glauconite and illite is not straightforward from both a chemical and a mineralogical point of view. Because the main difference between glauconite and illite is the weak or even absent 002 reflection in the glauconite XRD profile, due to a higher Fe content in the glauconite octahedral layers (Moore and Reynolds, 1997), it is rather difficult to detect glauconite by XRD. Although there is no direct evidence of the presence of glauconite in our samples, we cannot exclude it. In fact, a detailed analysis of clay minerals shows that mixed-layered clays are present in the GCL (Fig. F3), although in small amounts. These mixed-layered clays consist mainly of illite-smectite (IS) and chlorite-smectite (CS). We are able to estimate the content of Fe-rich mica at ~80%–85% and of chlorite at 75%–80% in GS and CS, respectively (Moore and Reynolds, 1997).

Bulk Inorganic and Organic Geochemistry

Concentration of the different phosphorus sedimentary phases and ferric iron are reported in Table T3. Fe-bound P and authigenic P are the most abundant phases, and their concentrations average 0.11 and 0.3 mg/g, respectively. Detrital P and organic-bound P are generally low, averaging 0.043 and 0.07 mg/g, respectively (Table T3). Ferric iron is present in relatively high quantities, averaging 2 mg/g. XRF results are

T3. Physical and chemical data, p. 20.

F3. Diffractograms of two samples, p. 14.



shown in Table T4, and only few analyzed elements display important variations between normal sediments and GCLs. On the whole, GCLs bear higher concentrations of iron, nickel, and potassium compared to host sediments, whereas the latter are characterized by slightly higher amounts of authigenic P, CaO, barium, and strontium (Tables T3, T4). Rock-Eval data indicate that GCLs contain lesser amounts of organic carbon, which averages 0.26 wt% in GCLs and 0.34 wt% in host sediments.

Spatial and Temporal Distribution of GCLs: Statistical Analysis

We have interpolated the age for each GCL at meters composite depth using the shipboard splices and age models, and thus have a complete record of GCLs for each of the studied sites. The GCL's time distributions are represented in Figure F4. On average, eight GCLs per 20 k.y. are recorded in the studied sites (corresponding to 2.5 occurrences per thousand years), and peaks of more than 10 occurrences per 20 k.y. are observed at Site 1143. Generally, GCLs are more recurrent in the upper part of the sequence. Sites 1143 and 1148 present the most continuous records of GCLs (Fig. F4).

All records were tested for randomness, using χ^2 statistics, in order to assess if patterns or trends in the temporal distribution of GCLs exist. For all sites except Site 1143, the results indicate that GCLs are not distributed randomly in time (Table T5). A trend in the length of the intervals between GCL events is observed for Sites 1145 and 1146, with intervals becoming shorter toward the upper part of the sequence (Fig. F5). At Site 1148 it is possible to detect a cyclicity. We executed autocorrelation analysis on the detrended records of intervals between events, and positive peaks on the autocorrelrogram were statistically significant only for Site 1148 (at 80% and 90% level of confidence) (Fig. F6). These peaks are located at 127, 140, 204, 270, and 477 k.y. Spectral analysis of GCL records from the other sites did not highlight any statistically significant cyclicity.

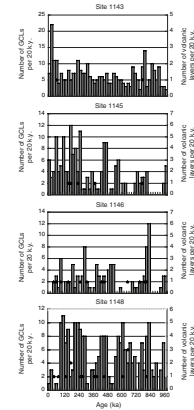
DISCUSSION

Many theories on the origin of green-colored layers have been brought forth, and the most common one is to attribute their genesis to diagenetic alteration of volcanic material. Gardner et al. (1986) suggested that the pale green laminae found on sediment from the Lord Howe Rise east of Australia were the product of alteration of volcanic material, as their occurrence correlated with the distribution of volcanic material and their mineralogy corresponded to bentonitic material. Lind et al. (1993) described colored bands from the Ontong Java Plateau sediments of Oligocene to Pleistocene age. They assigned a diagenetic origin to the laminae, as the colored bands crosscut bioturbation. No correlation between colored bands and proxies of productivity and climate was found, but their temporal distribution parallels the distribution of laminae observed at the Lord Howe Rise. Thus, Lind et al. (1993) ascribed their formation at the diagenetic alteration of volcanic material, as suggested by Gardner et al. (1986).

The origin of green granules on the Vietnam shelf was, on the other hand, attributed to diagenetic alteration of terrigenous material brought by the Mekong River into the SCS (Markov et al., 1996). These

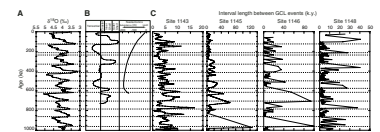
T4. XRF and Rock-Eval data, p. 22.

F4. Distribution of volcanic ash layers and GCLs in the SCS, p. 15.

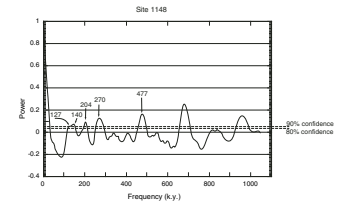


T5. Poisson distribution of GCLs, p. 23.

F5. Oxygen isotopes and neotectonics vs. GCL intervals, p. 16.



F6. Autocorrelrogram of GCL intervals, Site 1148, p. 17.



granules are mainly formed in nearshore environments characterized by low-energy sedimentation conditions. Quartz, feldspars, and clay minerals such as chlorite and micas are present in these sediments. Once settled in marine sediments, reducing conditions due to relatively high contents of organic matter altered the clay minerals, producing the characteristic green color.

There are few points against the volcanic origin for the GCLs recovered in the SCS. The distribution of volcanic layers found in the sediments from the SCS (Fig. F4) shows no striking similarity with the occurrences of GCLs. Several volcanic ash layers intercalated with GCLs were observed throughout the sediments during Leg 184, and, generally, no sign of green color was detected and the volcanic glass was unaltered. Moreover, green layers did not crosscut preexisting sedimentary features and were generally thicker (up to 3 cm vs. a few millimeters) than the colored bands found by Lind et al. (1993). Both Lind et al. (1993) and Gardner et al. (1986) did not notice any remarkable distinction between the colored layers and the matrix. Despite the overall variability of the measured parameters (see Table T3), it is still possible to detect some differences between GCLs and the host sediments: GCLs are relatively richer in iron, nickel, potassium, chlorite, smectite, and mixed-layered clays and are depleted in carbonate, authigenic P, barium, and strontium (Tables T3, T4).

We may explain the differences between GCL and host sediment composition, invoking diagenetic alteration of original detrital material (e.g., glauconitization) as the main process influencing the genesis of GCLs. SCS sediments are mainly constituted by nannofossil ooze mixed with detrital material rich in micas, quartz, and kaolinite. Relatively high contents of organic carbon, generally higher than 0.2 wt% in the investigated sections with peaks up to 1.2 wt%, are reported in SCS sediments recovered during Leg 184 (Wang, Prell, Blum, et al., 2000). These values are higher than the values reported for the Ontong Java Plateau sites, which average 0.1 wt% (Lind et al., 1993).

Reducing microenvironments could have formed close to the water/sediment interface. The active chemical exchange at the water/sediment interface is considered essential for the complete development of the glauconitization process (Chamley, 1989; Odin, 1988). The few observations of GCLs at Site 1144 in the northern margin of the SCS may, in fact, depend on the extremely high sedimentation rates that characterize this location (Table T1); such sedimentation rates would hasten the burial of sediments, impeding the chemical exchange between the seawater and the sediments. Moreover, redeposition processes and focused sedimentation (Wang, Prell, Blum, et al., 2000) could have disrupted the GCLs, making their detection difficult (Berger and Lind, 1997).

Increased microbial activity in the reducing microenvironments could have favored the degradation of organic matter, which is generally depleted in the GCLs compared to the surrounding matrix. These conditions lead to the dissolution of carbonates, which may explain the observed decreases of CaO, barium, and strontium in GCLs, normally associated with carbonates in marine sediments. Clays are altered, and mixed-layered clays are present in the sediments (Fig. F3). Iron is present at higher concentrations, bound both to silicates and to sulfides. Iron in a reduced form is responsible for the characteristic green color that disappears under oxygen-rich conditions.

The existence of a reducing environment during GCL formation is also attested to by relatively high concentrations of nickel that, being

chalcophile, tends to bind to iron sulfides. Another indication of reducing conditions is given by low amounts of authigenic P, which is mainly constituted by carbonate fluorapatite (CFA). The precipitation of CFA in marine sediments is dependent on many factors such as pore water concentrations of dissolved phosphate, oxygen content, and alkalinity (Jarvis et al., 1994). Degradation of organic material is the primary source of dissolved phosphate, but with high carbonate alkalinity of pore waters, CFA cannot precipitate (Jarvis et al., 1994; Krajewski et al., 1994).

The extent of glauconitization normally depends on the nature and grain size of the original material (Odin, 1988; Chamley, 1989). The presence of very fine grained particles, as is the case for sediments from the SCS, allows glauconitization to proceed only to the very first stage of the transformation, where glauconite has not appeared yet but some differences between the altered material and the host sediments have already become evident (Odin, 1988). Despite the fact that the SCS could be a suitable environment for verdine formation (Kronen and Glenn, 2000), this authigenic green clay mineral that develops in Fe-rich and shallow environments (between 5 and 60 m water depth) (Odin, 1988) has not been found in sediments recovered during Leg 184.

Glauconitization normally occurs at shallow depths, but the existence of glauconitic layers has already been reported in deeper waters (between 2000 and 3000 m water depth), comparable to SCS site locations (Chamley, 1989). We cannot exclude the possibility, considering the depth of the sites and the nature and geometry of the GCL, that they represent reworked material (i.e., distal turbidites) that have already undergone glauconitization or the higher porosity of which could have promoted glauconitization. Indeed, turbidites and reworked material have been reported at all Leg 184 sites (Wang, Prell, Blum, et al., 2000).

Many authors have used the distribution of glauconitic levels to indicate sea level changes over time (Chamley, 1989), as transgression and regression cycles can expose sediments located at different depths to conditions favorable to glauconitization. All sites except Site 1143 are characterized by nonrandom distribution of GCLs, and a trend in the length of intervals between successive GCL events is evident especially for Sites 1145 and 1146 (Table T5; Fig. F5). Comparison of these trends with the neotectonic curve calculated for the SCS northern margin (Lüdmann et al., 2001) indicates that since 600 ka, when the northern margin started uplifting, the frequency of GCLs was increased (Fig. F5). This observation supports the hypothesis of the reworked nature of the GCL, as tectonic activity and uplift may have increased the frequency of earthquakes and turbidites. Several foraminifer turbidites were observed at all SCS sites, and the relatively higher porosity of these turbidites (see Wang, Prell, Blum, et al., 2000) could have favored active fluid circulation in the sediments, promoting diagenetic alteration of the original material.

A correlation, although poor, seems to exist between interglacial periods characterized by high sea level and longer intervals between GCL events (Fig. F5), especially for Site 1143. This site is located close to the Sunda shelf, a region particularly sensitive to sea level changes (Pelejero et al., 1999). The temporal distribution of GCLs and the results of the autocorrelation point to cyclicity only at Site 1148, with frequencies close to values of primary frequencies and heterodynes of eccentricity. It is difficult to assess if this analysis bears reliable information: we are

aware of the uncertainties in the temporal distribution of the GCLs, which arise mainly from difficulties in the visual recording process of the layers (i.e., subjectivity of the different operators in defining a layer) and from the preliminary age models used in the analysis. Moreover, the spectral analysis did recover only the peak at 127 k.y., which is relatively close to a primary eccentricity frequency (e.g., peak at 123.8 k.y.); otherwise, only heterodynes of eccentricity have been observed. Nevertheless, we cannot exclude that changes in sea level resulting from the combination of climatic changes and tectonism could have had any influences on the distribution and genesis of the layers. We know that during the last glaciation the shelf surrounding the SCS was almost completely exposed (Pelejero et al., 1999). Therefore, during low sea level periods the zone of active glauconitization may have moved offshore, and as conditions at the sites became more favorable to diagenetic alteration the intervals between GCLs became shorter. Moreover, during regression and low sea level, turbidites were likely to be more frequent, thus supporting the hypothesis of the possible reworked nature of the GCLs.

CONCLUSIONS

Green clay layers in sediments from the SCS may result from the diagenetic alteration of the original detritus brought in from the Asian continent. The geometric relation to the host sediments and the differences, though small, in mineralogy, grain size, and geochemistry between the GCLs and the background sediments seem to favor the hypothesis that these layers represent the outcome of initial steps of glauconitization. Relatively high organic carbon content possibly set up localized reducing microenvironments, which started the glauconitization process. No striking evidence exists that points to a volcanic origin of the initial material. The temporal distribution of GCLs, although probably biased during the recording process on board, shows interesting correspondence to sea level and neotectonism curves, pointing to a possible influence of eustatism on the formation of the layers. Changes in the depth of the active glauconitization process and frequent turbidites, which provided material to the sites, are, in fact, the two most likely responsible processes.

We are far from having deciphered the ultimate process responsible for the formation of GCLs, but considering their widespread distribution in the ocean sediments and the possible amount of information they may bear, related to factors such as eustatism, climate, and tectonism, the complete understanding of their nature and genesis may require further investigation.

ACKNOWLEDGMENTS

The authors thank the captain, crew, and technical staff of ODP Leg 184 for assistance and help in obtaining samples. We gratefully acknowledge the scientific party for providing the stratigraphy for all sites. The authors sincerely thank G. Galetti (University of Fribourg, Switzerland) for XRF analyses and E. Verrecchia (University of Neuchâtel, Switzerland) for help on statistical treatment of the data set. Thanks also to J. Richard for technical assistance in preparing samples. Helpful reviews and comments from I.L. Fabricius, C. Robert, P. Blum, and D.

Rea helped improve the paper. This research used samples and data provided by the Ocean Drilling Program (ODP). ODP is sponsored by the U.S. National Science Foundation (NSF) and participating countries under management of Joint Oceanographic Institutions (JOI), Inc. This work was financially supported by the University and the Geological Institute of Neuchâtel (Switzerland).

REFERENCES

- Anderson, L.D., and Delaney, M.L., 2000. Sequential extraction and analysis of phosphorus in marine sediments: streamlining of the SEDEX procedure. *Limnol. Oceanogr.*, 45:509–515.
- Berger, A., and Loutre, M.F., 1991. Insolation values for the climate of the last 10 million years. *Quat. Sci. Rev.*, 10:297–317.
- Berger, W.H., and Lind, I.L., 1997. Abundance of color bands in Neogene carbonate sediments on Ontong Java Plateau: a proxy for sedimentation rate? *Mar. Geol.*, 144:1–8.
- Chamley, H., 1989. *Clay Sedimentology*: Berlin (Springer-Verlag).
- Espitalié, J., Deroo, G., and Marquis, F., 1986. La pyrolyse Rock-Eval et ses applications, Partie III. *Rev. Inst. Fr. Pet.*, 41:73–89.
- Gardner, J.V., Nelson, C.S., and Baker, P.A., 1986. Distribution and character of pale green laminae in sediment from Lord Howe Rise: a probable late Neogene and Quaternary tephrostratigraphic record. In Kennett, J.P., von der Borch, C.C., et al., *Init. Repts. DSDP*, 90 (Pt. 2): Washington (U.S. Govt. Printing Office), 1145–1159.
- Greenberg, A.E. (Ed.), 1995. *Standard Methods for the Examination of Water and Wastewater* (19th ed.): Washington (Am. Public Health Assoc.).
- Jantschik, R., Nyffeler, F., and Donard, O.F.X., 1992. Marine particle size measurement with a stream-scanning laser system. *Mar. Geol.*, 106:239–250.
- Jarvis, I., Burnett, W.C., Nathan, Y., Almbaydin, F.S.M., Attia, A.K.M., Castro, L.N., Flicoteaux, R., Hilmy, M.E., Husain, V., Qutawnah, A.A., Serjani, A., and Zanin, Y.N., 1994. Phosphorite geochemistry: state-of-art and environmental concerns. *Eclogae Geol. Helv.*, 87:643–700.
- Krajewski, K.P., Van Cappellen, P., Trichet, J., Kuhn, O., Lucas, J., Martin-Algarra, A., Prévot, L., Tewari, V.C., Gaspar, L., Knight, R.I., and Lamboy, M., 1994. Biological processes and apatite formation in sedimentary environments. *Eclogae Geol. Helv.*, 87:701–745.
- Kronen, J.D., Jr., and Glenn, C.R., 2000. Pristine to reworked verdine: keys to sequence stratigraphy in mixed carbonate-siliciclastic foreereef sediments (Great Barrier Reef). In Glenn, C.R., Prévôt-Lucas, L., and Lucas, J. (Eds.), *Marine Authigenesis: From Global to Microbial*. Spec. Publ.—SEPM, 66:387–403.
- Kübler, B., 1983. Dosage quantitatif des minéraux majeurs des roches sédimentaires par diffraction X. *Cah. Inst. Geol. Neuchâtel*, Ser. ADX, 1:12.
- Lafargue, E., Espitalié, J., Marquis, F., and Pillot, D., 1996. Rock-Eval 6 applications in hydrocarbon exploration, production and in soil contamination studies. Latin American Congress on Organic Geochemistry, Cancun. (Abstract)
- Lind, I.L., Janecek, T.R., Krissek, L.A., Prentice, M.L., and Stax, R., 1993. Color bands in Ontong Java Plateau carbonate oozes and chalks. In Berger, W.H., Kroenke, L.W., Mayer, L.A., et al., *Proc. ODP, Sci. Results*, 130: College Station, TX (Ocean Drilling Program), 453–470.
- Lüdmann, T., Wong, H.K., and Wang, P., 2001. Plio-Quaternary sedimentation processes and neotectonics of the northern continental margin of the South China Sea. *Mar. Geol.*, 172:331–358.
- Markov, Y.D., Mozherovskii, A.V., and Eiberman, M.F., 1996. Origin of clay granules in the South Vietnam shelf sediments, South China Sea. *Lithol. Miner. Resour.*, 31:311–318.
- Mix, A.C., Pisias, N.G., Rugh, W., Wilson, J., Morey, A., and Hagelberg, T.K., 1995. Benthic foraminifer stable isotope record from Site 849 (0–5 Ma): local and global climate changes. In Pisias, N.G., Mayer, L.A., Janecek, T.R., Palmer-Julson, A., and van Andel, T.H. (Eds.), *Proc. ODP, Sci. Results*, 138: College Station, TX (Ocean Drilling Program), 371–412.
- Moore, D.M., and Reynolds, R.C., 1997. *X-Ray Diffraction and the Identification and Analysis of Clay Minerals* (2nd ed.): Oxford (Oxford Univ. Press).

- Odin, G.S. (Ed.), 1988. *Green Marine Clays*: Amsterdam (Elsevier).
- Pelejero, C., Kienast, M., Wang, L., and Grimalt, J.O., 1999. The flooding of Sundaland during the last deglaciation: imprints in hemipelagic sediments from the southern South China Sea. *Earth Planet. Sci. Lett.*, 171:661–671.
- Ruttenberg, K.C., 1992. Development of a sequential extraction method for different forms of phosphorus in marine sediments. *Limnol. Oceanogr.*, 37:1460–1482.
- Supko, P.R., Perch-Nielsen, K., et al., 1977. *Init. Repts. DSDP*, 39: Washington (U.S. Govt. Printing Office).
- Wang, P., Prell, W.L., Blum, P., et al., 2000. *Proc. ODP, Init. Repts.*, 184 [CD-ROM]. Available from: Ocean Drilling Program, Texas A&M University, College Station, TX 77845-9547, USA.

Figure F1. Map of the South China Sea and location of the six sites drilled during ODP Leg 184. The thick dotted line indicates the continental/oceanic crust boundary, whereas the thin dotted line indicates the shelf limit.

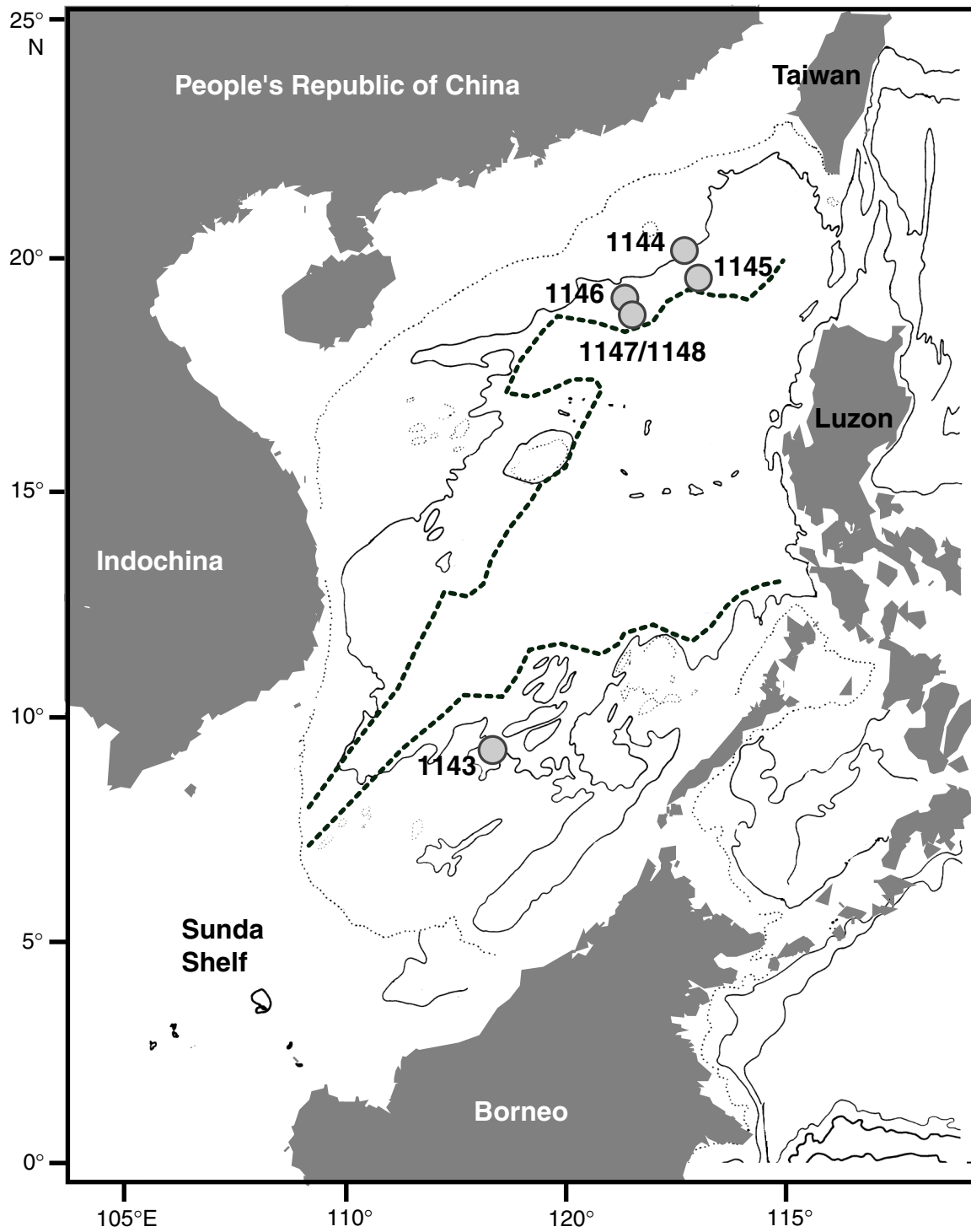


Figure F2. Samples used for this study. Solid arrows = green clay layer (GCL) samples, open arrows = background sediment samples. It is evident from this figure that not all the GCLs sampled are continuous.

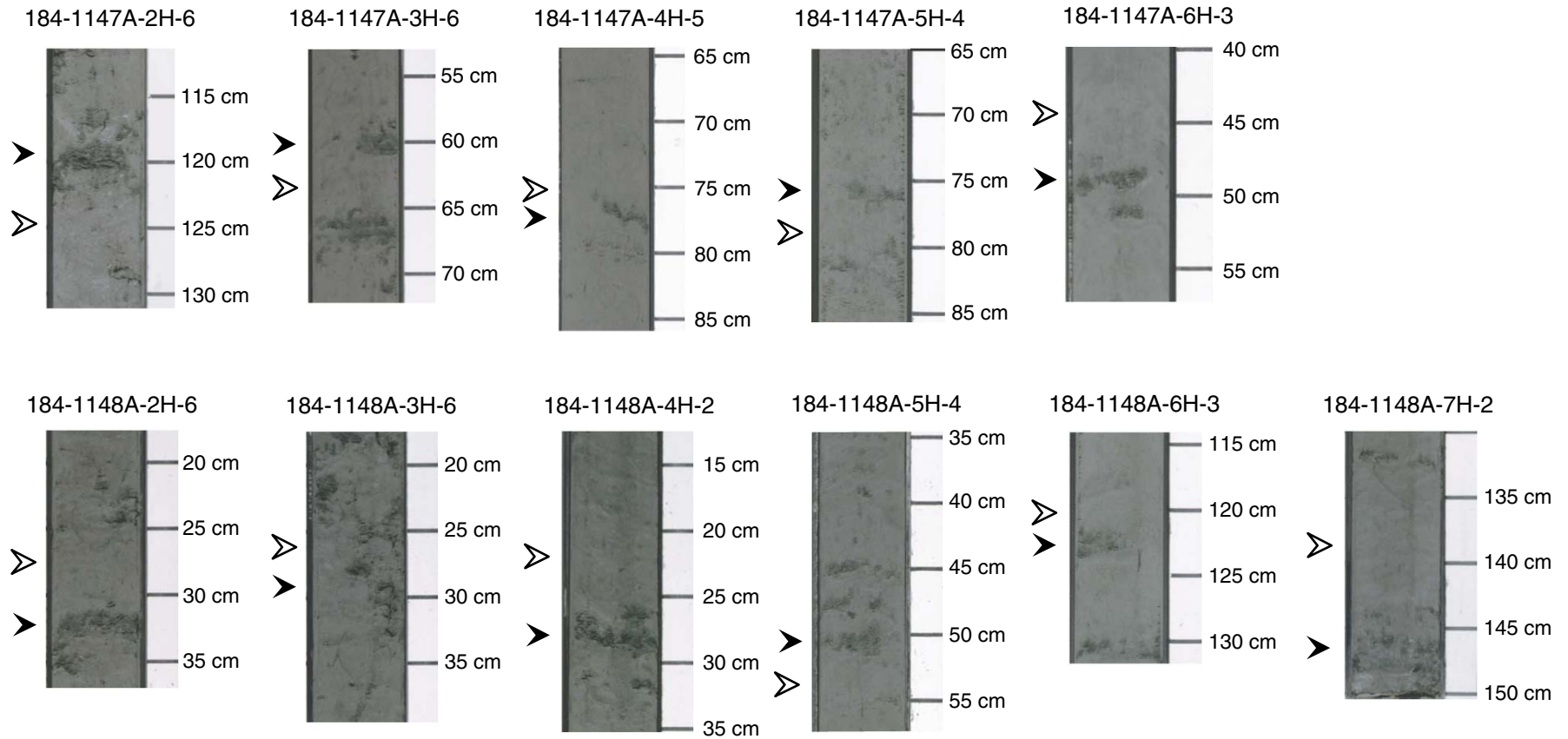


Figure F3. A. Diffractograms of Samples 184-1148A-3H-6, 25–27 cm (black line), and 3H-6, 28–30 cm (gray line), <2- μm glycolated fraction. B. Diffractograms of Samples 184-1148A-5H-4, 52–54 cm (gray line), and 5H-4, 49–51 cm (black line), <2- μm glycolated fraction. IS = illite/smectite, with 80%–85% of Fe-rich muscovite; CS = chlorite/smectite, with 75%–80% of chlorite. Mixed-layered clays are estimated as described in Moore and Reynolds (1997). sed. = sediment.

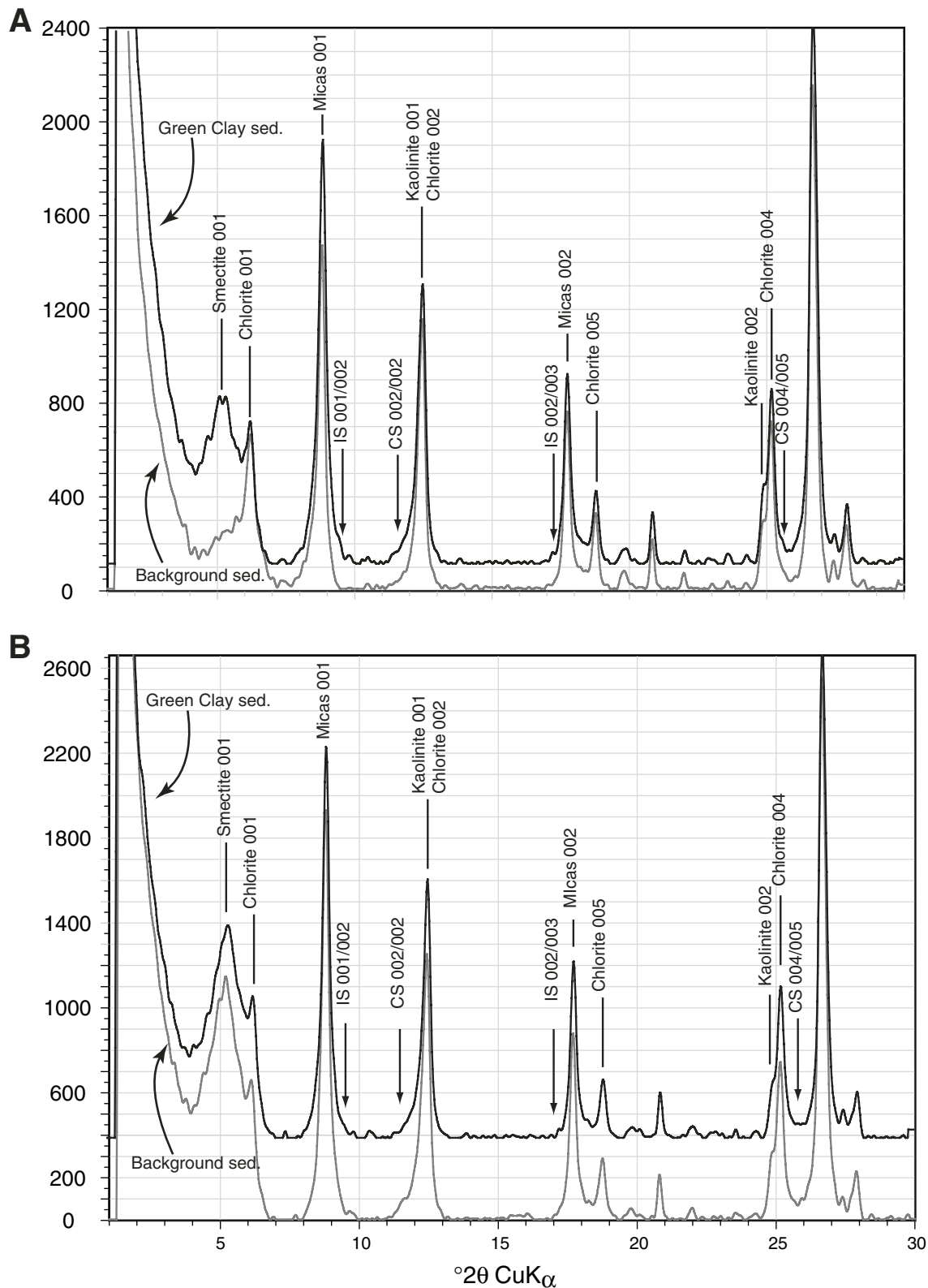


Figure F4. Temporal distribution of volcanic ash layers and green clay layers (GCLs) in the South China Sea spanning the last million years. Star = number of volcanic layers observed at all sites drilled during Leg 184, bar = number of GCLs recorded for each site.

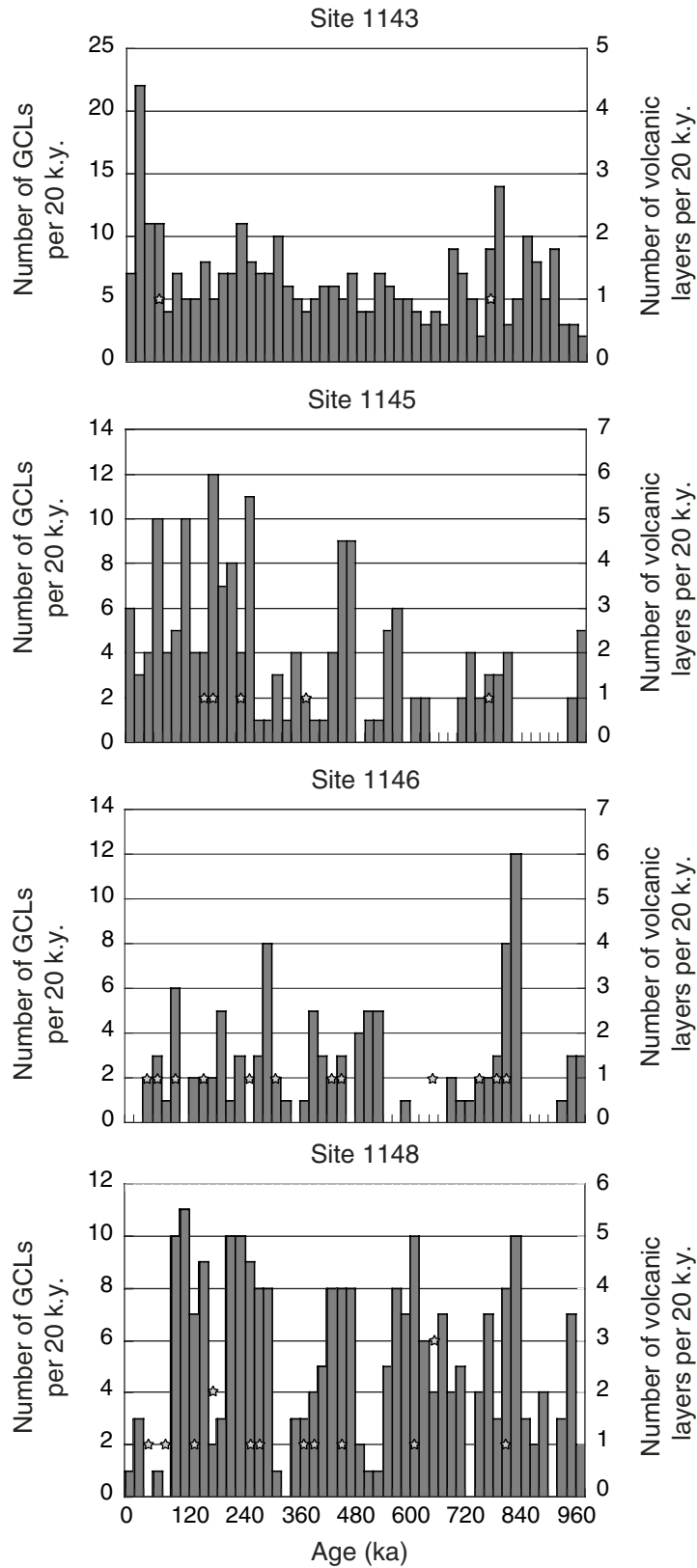


Figure F5. From the left, (A) oxygen isotopic curve of *Cibicidoides wuellerstorfi* from ODP Site 849, eastern equatorial Pacific (Mix et al., 1995), (B) neotectonics and relative sea level curves obtained by Lüdmann et al. (2001) from seismic data from the northern margin of the South China Sea, and (C) interval length between green clay layers (GCLs) at the investigated Leg 184 sites vs. time. The dotted lines indicate interglacial periods and in many cases correlate to longer intervals between GCL events (see text for explanation).

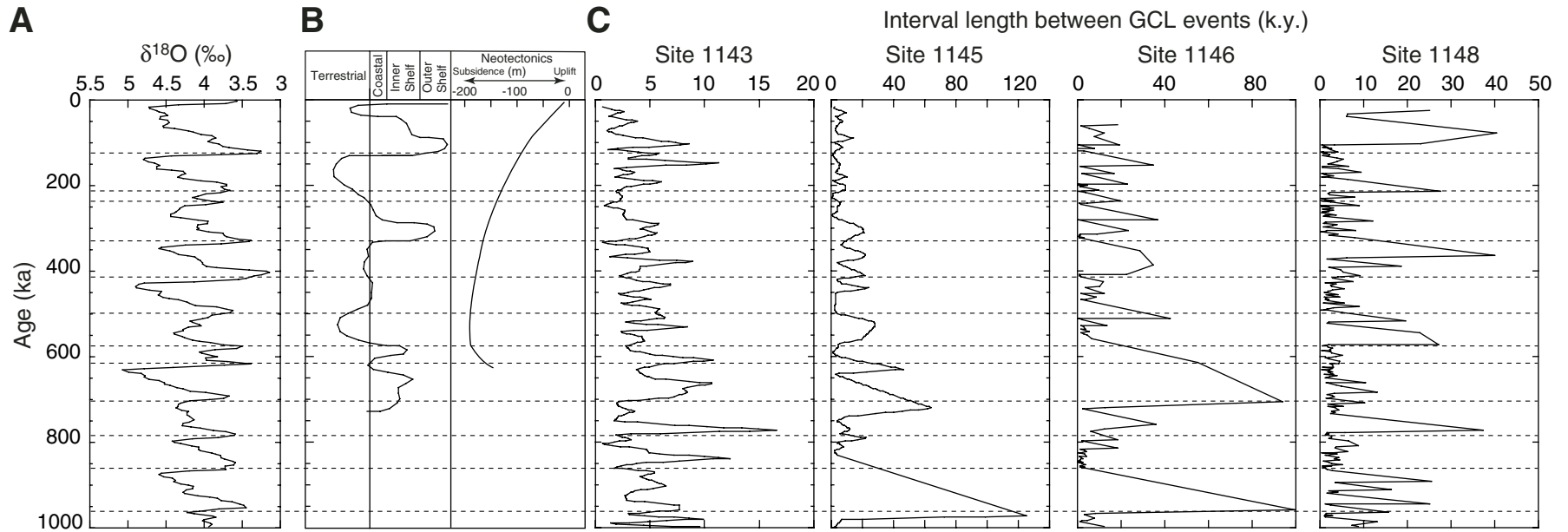


Figure F6. Autocorrelogram of interval lengths between green clay layers (GCLs) for Site 1148. The two dotted lines represent significance levels at 80% and 90%, calculated as $g = 1 - e[(\ln p - \ln m)/m - 1]$, where p = level of significance and $m = (\text{number of observations})/2$. The choice of relatively low significance levels was determined on the consideration that during onboard observation and recording of the GCLs, both continuous and bioturbated layers were counted. Signals at 127, 140, 204, 270, and 477 k.y. are statistically significant. Other peaks (frequencies >500 k.y.) were not taken into account because they were statistically insignificant. Values of 140, 204, and 477 k.y. are close to heterodynes (difference) of different eccentricity terms (Berger and Loutre, 1991).

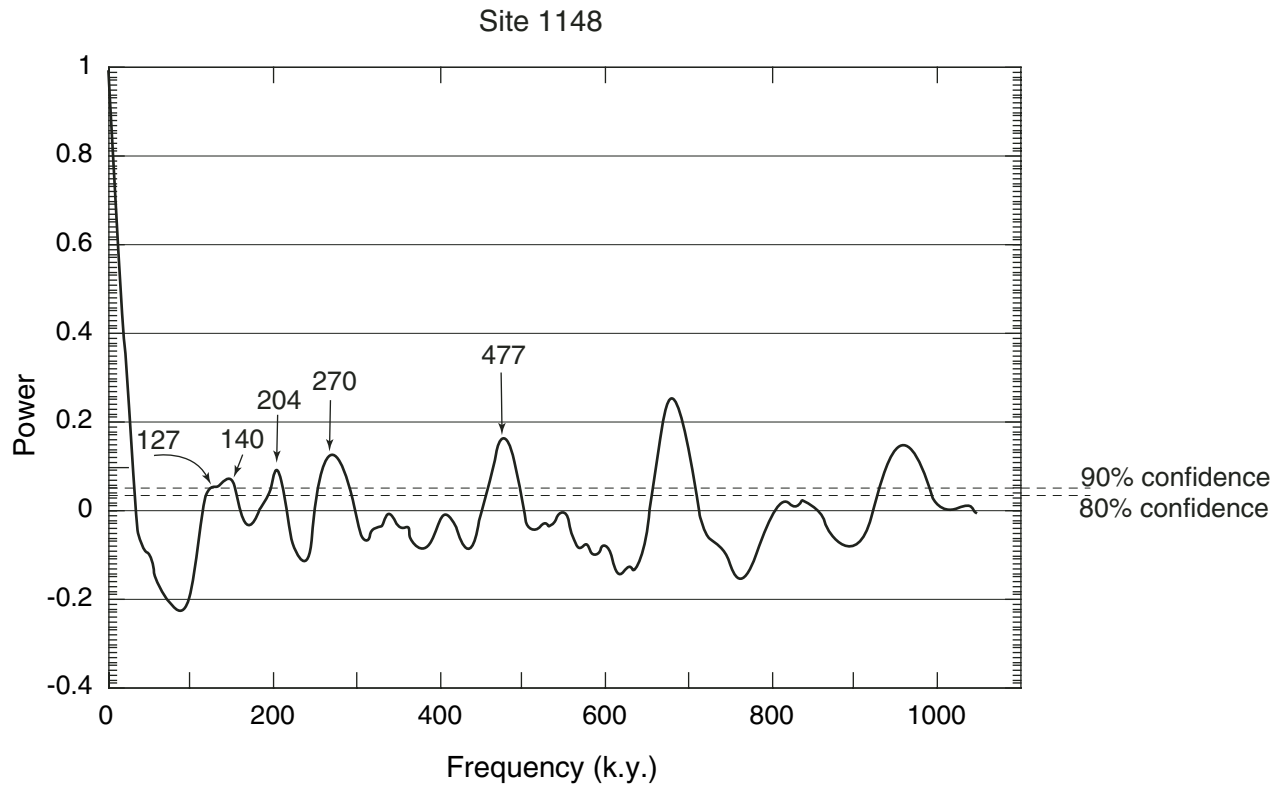


Table T1. Location of the studied sites.

Site	Latitude	Longitude	Water depth (mbsl)	Sedimentation rate (m/m.y.)
1143	9°21.72'N	113°17.11'E	2772	55
1144	20°3.18'N	117°24.14'E	2037	494
1145	19°35.04'N	117°37.86'E	3175	119
1146	19°27.40'N	116°16.37'E	2092	147
1147	18°50.11'N	116°33.28'E	3246	96
1148	18°50.17'N	116°33.94'E	3294	141

Note: Data are from Wang, Prell, Blum, et al. (2000).

Table T2. Depths and ages for green clay layers used for statistical analyses.

Depth (mcd)	Age (ka)
Site 1143	
0.780	16.548
0.810	17.070
0.870	17.768
0.900	18.098
0.930	18.425
1.010	19.290
1.035	19.559
1.080	20.054
1.260	21.972
1.415	23.628
1.430	23.787
1.590	25.494
1.625	25.873
1.900	28.800
2.050	30.427
2.050	30.427
2.125	31.210
2.130	31.264
2.145	31.423
2.160	31.578
2.165	31.636
2.255	32.605
2.430	34.491
2.445	34.658
2.615	36.465
2.645	36.795
2.670	37.070
2.765	38.106
2.880	39.297
3.150	42.250
3.180	42.568
3.230	43.096
3.290	43.717
3.350	44.350
3.675	47.825
3.990	51.221
4.095	52.345
4.305	54.629
4.575	57.525
4.695	58.823
4.915	61.196
5.065	63.092
5.125	63.862
5.325	66.339
5.445	67.835
5.565	69.341
5.650	70.396
5.675	70.710
5.945	74.092
6.295	78.461
6.405	79.838
6.475	80.946
6.605	86.057
6.650	88.253
6.760	93.580
6.925	101.540
7.190	111.080
7.225	111.500
7.330	112.760
7.470	114.440
7.495	114.740
7.590	115.880
7.965	120.380

Note: Only a portion of the table appears here. The complete table is available in [ASCII](#).

Table T3. GRA bulk density and porosity data, grain size, clay and bulk mineralogy, and Fe(ferric) and phosphorus sedimentary phases of selected samples. (Continued on next page.)

Core, section, interval (cm)	Depth		Age (Ma)	Thickness (cm)	Color	GRA (g/cm ³)	Porosity (%)	<8 μm (%)	>8 μm (%)	Clay mineralogy 2–16 μm (%)			Clay mineralogy <2 μm (%)			
	(msbf)	(mcd)								Micas	Kaolinite	Chlorite	Micas	Kaolinite	Chlorite	Smectite
184-1147A-																
2H-6, 124–126	14.14	15.59			Normal	1.453	74.3	92.5	7.5	50.9	4.7	44.4	40.5	5.5	27.5	26.6
2H-6, 118–120	14.08	15.53	0.17	1.86	Green	1.464	73.7	96.4	3.6	48.5	7.9	43.7	37.6	11.9	20.1	30.5
3H-6, 63–64	23.03	24.78			Normal	1.531	70.1	89.3	10.7	55.5	4.7	39.8	58.6	10.4	24.3	6.6
3H-6, 60–61	23.06	24.81	0.26	1.53	Green	1.483	72.7	86.0	14.0	51.2	6.3	42.5	49.4	10.0	24.1	16.5
4H-5, 75–76	31.15	34.1			Normal	1.476	73.1	95.0	5.0	57.0	4.3	38.7	63.2	11.7	25.1	miss
4H-5, 77–78	31.17	34.12	0.37	1.65	Green	1.459	74.0	90.9	9.1	58.0	4.4	37.6	59.3	10.5	28.9	1.4
5H-4, 78–79	39.18	42.08			Normal	1.483	72.7	88.9	11.2	54.3	8.5	37.2	65.8	9.8	23.3	1.1
5H-4, 76–77	39.16	42.06	0.50	0.88	Green	1.481	72.8	12.3	87.7	55.9	6.1	38.0	66.4	10.7	20.6	2.3
6H-3, 45–46	46.85	51.1			Normal	1.587	67.0	93.5	6.5	54.6	5.4	40.0	51.3	11.0	19.0	18.6
6H-3, 50–51	46.9	51.15	0.65	1.24	Green	1.578	67.5	82.1	17.9	53.4	5.9	40.8	34.1	9.7	30.8	25.4
2H-6, 26–28	8.56	13.41			Normal	1.487	72.5	92.6	7.4	51.1	2.3	46.6	46.9	11.4	21.2	20.6
2H-6, 31–33	8.61	13.46	0.19	1.74	Green	1.476	73.1	90.9	9.1	49.4	2.2	48.4	43.9	4.1	32.3	19.8
3H-6, 25–27	17.98	22.83			Normal	1.451	74.5	94.8	5.2	50.9	6.8	42.2	49.3	13.2	24.3	13.1
3H-6, 28–30	18.01	22.86	0.33	2.43	Green	1.434	75.5	91.6	8.4	50.1	7.2	42.8	50.0	6.0	22.8	21.2
4H-2, 22–24	21.52	26.37			Normal	1.474	73.2	92.4	7.6	49.1	4.5	46.4	miss	miss	miss	miss
4H-2, 27–29	21.57	26.42	0.38	2.67	Green	1.434	75.5	83.9	16.1	47.9	5.8	46.3	48.2	8.4	24.0	19.3
5H-4, 52–54	34.32	39.17			Normal	1.516	70.8	45.9	54.1	53.3	8.7	38.0	48.1	5.7	22.1	24.1
5H-4, 49–51	34.29	39.14	0.56	2.13	Green	1.527	70.2	89.3	10.7	52.4	7.2	40.5	47.3	7.4	23.0	22.3
6H-3, 119–121	42.99	48.79			Normal	1.599	66.0	75.8	24.2	52.4	11.3	36.3	40.6	9.9	20.9	28.6
6H-3, 121–123	43.01	48.81	0.70	1.71	Green	1.571	67.6	75.5	24.5	54.5	10.8	34.7	46.1	6.7	21.5	25.8
7H-2, 137–139	51.17	58.07			Normal	1.61	65.4	90.8	9.2	53.9	8.3	37.8	44.1	10.1	20.9	24.9
7H-2, 145–147	51.25	58.15	0.83	3.08	Green	1.576	67.4	89.1	10.9	53.7	7.8	38.6	58.0	13.6	23.8	4.6
				Average:	Green	1.50	71.82	80.7	19.3	52.3	6.5	41.2	49.1	9.0	24.7	18.4
					Normal	1.52	70.88	84.9	15.1	53.0	6.7	40.3	49.5	9.7	22.6	18.2

Notes: Depths and ages of green clay layers (GCLs) are interpolated using splices and age models provided in Wang, Prell, Blum, et al. (2000). Gamma ray attenuation (GRA) values of GCLs and background sediments are converted to porosity using the coefficient obtained from least-square regression of GRA (smoothed and sampled at all moisture and density intervals) against porosity (data in Wang, Prell, Blum, et al., 2000). miss = missing data.

Table T3 (continued).

Core, section, interval (cm)	Depth		Age (Ma)	Thickness (cm)	Bulk mineralogy (%)						Sedimentary phosphorous phases (mg/g)				
	(msbf)	(mcd)			Phyllosilicates	Quartz	K-feldspar	Plagioclase	Calcite	Pyrite	Fe	Fe bound	Authigenic	Detrital	Organic bound
184-1147A-															
2H-6, 124–126	14.14	15.59			20.0	9.7	1.1	2.8	15.3	1.0	1.23	0.13	0.31	0.03	0.07
2H-6, 118–120	14.08	15.53	0.17	1.86	25.5	11.4	2.1	3.0	9.9	0.9	4.39	0.28	0.22	0.03	0.08
3H-6, 63–64	23.03	24.78			25.3	17.1	1.7	5.1	3.2	0.6	2.38	0.28	0.52	0.04	0.07
3H-6, 60–61	23.06	24.81	0.26	1.53	11.8	9.4	1.0	2.3	0.6	0.4	6.93	0.06	0.24	0.06	0.09
4H-5, 75–76	31.15	34.1			15.1	15.9	1.5	4.0	6.0	0.8	2.63	0.05	0.21	0.04	0.08
4H-5, 77–78	31.17	34.12	0.37	1.65	15.2	15.9	1.2	4.3	6.1	0.8	3.54	0.03	0.25	0.04	0.07
5H-4, 78–79	39.18	42.08			16.8	13.3	1.1	2.4	15.0	0.8	1.78	0.06	0.34	0.04	0.06
5H-4, 76–77	39.16	42.06	0.50	0.88	18.2	13.3	1.6	3.0	12.2	0.8	3.44	0.07	0.21	0.05	0.07
6H-3, 45–46	46.85	51.1			13.2	12.0	1.0	3.1	10.9	0.6	1.18	0.11	0.37	0.04	0.06
6H-3, 50–51	46.9	51.15	0.65	1.24	14.2	14.1	1.2	3.8	10.3	0.7	3.23	0.11	0.20	0.05	0.07
2H-6, 26–28	8.56	13.41			14.5	8.3	1.6	3.0	1.7	0.5	1.34	0.06	0.20	0.04	0.07
2H-6, 31–33	8.61	13.46	0.19	1.74	19.3	11.7	1.0	3.4	1.7	0.6	2.37	0.07	0.24	0.04	0.07
3H-6, 25–27	17.98	22.83			16.0	16.4	1.4	3.2	1.1	0.5	2.63	0.04	0.29	0.04	0.08
3H-6, 28–30	18.01	22.86	0.33	2.43	16.8	11.3	1.5	5.5	1.2	0.6	2.14	0.04	0.20	0.04	0.07
4H-2, 22–24	21.52	26.37			20.0	17.8	1.3	4.4	4.4	0.8	1.76	0.04	0.57	0.04	0.07
4H-2, 27–29	21.57	26.42	0.38	2.67	23.0	11.5	1.7	3.4	1.0	0.5	4.46	0.37	0.35	0.04	0.07
5H-4, 52–54	34.32	39.17			19.4	14.9	1.0	4.5	4.6	0.6	1.60	0.09	0.42	0.04	0.07
5H-4, 49–51	34.29	39.14	0.56	2.13	17.5	15.5	1.3	4.8	1.9	0.6	2.28	0.18	0.33	0.04	0.06
6H-3, 119–121	42.99	48.79			13.0	10.3	0.7	2.3	9.6	0.6	1.36	0.10	0.58	0.04	0.06
6H-3, 121–123	43.01	48.81	0.70	1.71	13.6	10.4	2.3	2.7	11.0	0.5	1.44	0.08	0.21	0.07	0.06
7H-2, 137–139	51.17	58.07			12.9	11.8	0.8	3.0	3.6	0.4	1.44	0.05	0.39	0.04	0.07
7H-2, 145–147	51.25	58.15	0.83	3.08	17.0	10.0	1.0	2.7	1.7	0.5	3.24	0.06	0.23	0.05	0.09
				Average:	17.5	12.2	1.4	3.5	5.2	0.6	3.405	0.124	0.244	0.047	0.074
					16.9	13.4	1.2	3.5	6.9	0.6	1.661	0.101	0.379	0.04	0.067

Table T4. Results of XRF and Rock-Eval analyses performed on four selected samples.

Hole:	184-1148A-			
Core, section, interval (cm):	2H-6, 26-28	2H-6, 31-33	6H-3, 119-21	6H-3, 121-123
Color:	Normal	Green	Normal	Green
Major element oxides (wt%):				
SiO ₂	56.76	56.04	47.10	47.15
TiO ₂	0.66	0.68	0.66	0.64
Al ₂ O ₃	16.66	16.50	15.09	14.84
Fe ₂ O ₃	3.11	4.48	4.19	4.38
FeO	2.22	2.09	1.86	1.87
MnO	0.14	0.17	0.29	0.28
MgO	2.72	2.87	2.90	2.91
CaO	2.54	2.08	9.36	9.28
Na ₂ O	3.32	3.28	2.15	2.12
K ₂ O	3.25	3.28	2.65	2.68
P ₂ O ₅	0.12	0.11	0.16	0.14
LOI (wt%):	8.15	8.12	13.70	13.61
Total (wt%):	99.65	99.71	100.11	99.90
Trace elements (ppm):				
Ba	890	864	553	528
Cr	74	77	78	81
Cu	96	74	18	16
Nb	12	13	12	12
Ni	69	80	58	63
Pb	<7	<7	<7	<7
Rb	140	143	113	118
Sr	215	191	389	385
V	134	130	124	124
Y	26	27	26	25
Zn	113	123	100	98
Zr	141	141	133	133
Total:	0.19	0.19	0.16	0.16
Fe total (%):	5.58	6.81	6.26	6.46
TOC (wt%):	0.43	0.29	0.25	0.24

Notes: LOI = loss on ignition, TOC = total organic carbon. Fe total = Fe₂O₃. XRF = X-ray fluorescence. Bold entries are major element oxides and trace elements used in the text to underline differences between GCL and host sediments.

Table T5. Parameters used in testing for Poisson distribution (randomness) of green layers.

Site	Period (k.y.)	<i>N</i> intervals	<i>N</i> green layers	<i>N</i> classes	Degrees of freedom	Calculated χ^2	χ^2 (5% level of significance)
1143	0–1105	221	345	7	4	4.553	9.488
1145	0–1005	201	171	6	3	32.967	7.815
1146	0–860	200	108	5	2	32.757	5.991
1148	0–1085	217	252	6	3	14.166	7.815

Notes: Only for Site 1143 we fail to reject the null hypothesis (green layers follow a Poisson random distribution). For the other sites, we have to reject randomness. Δt interval = 5 k.y. *N* = number.